Experimental study of the effect of water vapor on dynamics of a high electric field non-equilibrium diffuse discharge in air

Alexandra Brisset, Pierre Tardiveau, Kristaq Gazeli, Blandine Bournonville, Pascal Jeanney, Karim Ouaras, Lionel Magne, Stéphane Pasquiers

Experimental study of the effect of water vapor on dynamics of a high electric field non-equilibrium diffuse discharge in air

Experimental study of the effect of water vapor on dynamics of a high electric field non-equilibrium diffuse discharge in air

A. Brisset[1], P. Tardiveau[1], K. Gazeli[1], B. Bournonville[1], P. Jeanney[1], K. Ouaras[1], L. Magne[1], S. Pasquiers[1]

[1] *Université Paris-Saclay, CNRS, Laboratoire de Physique des Gaz et des Plasmas, 91405 Orsay, France*

Abstract: We report results on the influence of relative humidity on the propagation speed, the intensity of the emitted light, the energy and the gas temperature of a pin-to-plane nanosecond pulsed discharge at atmospheric pressure in synthetic air. The discharge is generated under very high overvoltage (several tens of kV) so that it propagates with a voluminous, diffuse, and stable pattern. It is shown that the water vapor content has a strong impact on the discharge dynamics for gas mixtures with high relative humidity and for the highest electric field values. In particular, for voltage pulse amplitudes higher than 65 kV and relative humidity higher than 30%, the propagation abruptly slows down and the light intensity profiles show a stronger emission at the pin which weakens in the rest of the gap. The electric energy is slightly lower in humid air, independently of water vapor concentration. Also, time and spatially resolved gas temperature measurements carried out for different voltages show a late and significant heating at the pin whatever the water vapor content. An evaluation of the energy consumed in fast heating processes is proposed, showing an increased energy consumption at the pin in highly humid air. Besides, the hypotheses allowing for the consideration of the rotational temperature of the second positive system of nitrogen (N_2(SPS)) as the gas temperature under high electric field conditions are discussed.

Keywords: Non-equilibrium plasma, atmospheric air discharge, diffuse discharge, nanosecond discharge, humidity effects, fast imaging, optical emission spectroscopy

1. Introduction

Voluminous and diffuse non-equilibrium electric discharges generated in air at atmospheric pressure can be created in pin-to-plane electrode gaps when applying a very high overvoltage (several tens of kV) at sub-nanosecond time scales. Under those conditions, the global appearance of the discharge is unusual: it is not filamentary and randomly branched as it would be for classical streamer discharges, but instead it is stable in space and time showing a diffuse light emission over a much larger volume (1.5 cm^3).

The physics of the diffuse discharge is not fully understood and only a few works describe its features and propose explanations for its unique behavior [1-5]. It deviates somehow from the commonly accepted classical streamer concepts [6-9] and it differs from the so-called nanosecond discharges largely investigated under moderate voltages (up to few tenths of kV) [10-12]. Under negative polarity conditions, the characteristics of high electric field diffuse discharges are often associated to fast (or runaway) electrons inducing X-ray emission from the anode plane [13]. Those mechanisms have been largely investigated experimentally and detailed through theoretical studies [14-17]. The situation is not the same under positive polarity where the production of runaway electrons is unlikely because of space charge building. However, in the early stages of the inception of the discharge and propagation from the pin, the overvoltage quickly leads to very intense applied electric fields, higher than 1 MV/cm, and the shielding driven by the growing streamer space charge becomes less efficient. Field strengths could be still suitable for runaway electrons generation [18-20]. The X-photons subsequently emitted from the anode pin can induce a type of extended self-preionization of the gas in the gap and the formation of a diffuse discharge. The dynamics of development itself may be modified, the space charge being much more distributed in space and the field increasing above the ionization threshold in the plasma channel left behind the streamer front [21, 22]. The electric field remains at a high level in the whole gap as long as the voltage is applied. The width of the voltage pulse has to be short enough (no more than a few tenths of ns) to limit the discharge current and to prevent from excessive heating of the gas.

The extreme overvoltage applied to the pin, tens of kilovolts, results in a global field intensification on air volumes and time periods much larger than in a classical low voltage streamer scheme. Excitation, ionization and dissociation mechanisms can be strongly enhanced which makes the design of large and almost homogeneous atmospheric air plasma reactors suitable for many applications. For air pollution control purposes, high densities of reactive species can be reached in the diffuse discharge and can promote the abatement efficiency of chemical processes. The low gas temperature of the discharge, close to the ambient one or slightly higher, also limits the production of harmful nitrogen oxides and the energy consumption. A recent experimental study on OH radicals produced by a diffuse discharge in humid air under 85 kV pulses shows that a maximum density of 2.10^{16} cm^{-3} can be reached near the pin for a specific energy density of 40 $J.L^{-1}$ [23]. The mean energy efficiency of OH production is estimated to be about 1.5 molecules / 100 eV for 1% of water vapor in air, which is significantly higher than the production efficiency of other types of discharges. That work also stressed out qualitatively that the content of water vapor could change significantly the discharge characteristics. Previous studies already demonstrated that the addition in air of low concentrations of other molecules (such as polluting or flammable species) strongly influences the propagation and the energy deposition of similar high field diffuse discharges [24]. For 1.5% of propane or heptane in air, such discharges become filamentary and the injected energy density gets localized into the filaments. The absorption of UV and/or X-rays by hydrocarbons over shorter distances than those in pure air has been considered to explain the discharge modifications, limiting the preionization mechanism previously mentioned. Based on the above, the purpose of the present work is to study the effects of water vapor content on the high electric field diffuse discharge dynamics through the quantification of its propagation speed, gas temperature and energy deposition. This investigation is expected to bring new insights to the mechanisms that drive the discharge under high electric fields.

Numerous studies describe the effects of the humidity on the electrical properties of streamer discharges in low or moderate external field conditions [25-32]. Most of them face issues related to partial discharge formation on dielectric surfaces which affect the electrical insulation or to the understanding of leader formation processes with streamers propagating in long atmospheric air gaps. Experimental works usually focus on how humidity influences the inception or breakdown voltage and the field stability in the discharge process. It is generally described that breakdown occurs at higher voltages if humidity increases. This is partly due to the inhibiting effect of water clusters on electron detachment processes, which delays the occurrence of seed electrons in the air gap. It is also related to the increase in the rate of three body attachment [33, 34] or dissociative recombination [35] with complex clustered ions, depending on the electron density. In the streamer plasma channel, it results in a decrease of the conductivity and electrical charges injection. The space charge and the field at the streamer head are then lower and, as a consequence, stronger external fields are required to achieve breakdown at higher humidity levels. In high field regions like the streamer head, the effect of humidity on attachment is not significant since ionization rate by electron impact is still much higher. However, water vapor content reduces the UV absorption length [36] and makes the photoionization process somehow less efficient in front of the streamer. For specific conditions of geometry or voltage characteristics [25], a decrease of breakdown voltage with humidity can be observed below a given threshold of water concentration (about 5 $g.m^{-3}$ for a 20 cm pin-to-plane gap under DC voltage). This opposite behavior is not clear but, in medium-sized air gaps with leader formation, it could be associated to the pre-formation of a glow discharge instead of a streamer. In the presence of insulating surfaces where condensation might take place, breakdown voltage also decreases with highest humidity levels [26].

The dependence of the inception voltage on the voltage rise rate in corona discharges in humid gases has been investigated by different authors. It is shown that the addition of water facilitates the inception of the discharge when the voltage rise time is long enough [27-29] and improves the stability of the discharge, as evidenced by the reduction of the dispersion of inception time and voltage distributions [29]. This latter effect has been explained in [30] by the assumption of O_2^- ion density dependence upon both humidity and electric field. Few studies investigated the effect of humidity on the propagation speed of streamer discharges. In a uniform external field arrangement with 12 cm gap electrode spacing [31], a 20% increase of the speed is observed with water vapor content increasing from 8 to 19 $g.m^{-3}$. This effect is accentuated when the electric field is stronger or when the pulsed voltage applied to the pin electrode that triggers the discharge (i.e. the energy provided for inception) is higher. A correlation between the streamer propagation velocity and the ratio of the applied field over the stability

field is given in [31], partly depending on the humidity level. A more recent study [32] gives contradictory results with a decrease of the velocity with increasing humidity, roughly explained by the increase of attachment and recombination coefficients with humidity. However, those results remain specific to corona discharges in air gaps of several tens of centimeters with voltage rise times of tens of microseconds, much longer than those used in our study.

Beyond those effects on the discharge electrical features, the humidity content also proved to have a significant impact on the discharge heating processes. It is observed that the streamer-leader transition in long air gaps is promoted when humidity is increased, partly due to water enhanced vibrational relaxation mechanisms of nitrogen and oxygen molecules. The relaxation rate can be increased by interactions between the vibrational modes of H_2O and those of N_2 and O_2. In [33], the time constant of the relaxation of $N_2(v = 1)$ is estimated to be reduced down to about 60 µs with 16 $g.m^{-3}$ of humidity and a gas temperature of 600 K instead of 300 µs at 4 $g.m^{-3}$. More recently, Komuro *et al.* [37] simulated the fast gas heating in a 13 mm gap pin-to-plane streamer discharge by considering those energy transfers. It is shown that only a small part of the energy of $N_2(v)$ is used for H_2O vibrational excitation and that humidity has a small effect on $O_2(v=1)$ relaxation up to 3 µs. However, fast gas heating in humid air is enhanced by V-T relaxation of H_2O vibrational modes with a time constant as low as 40 ns, as well as by fast exothermic formation of OH radicals. The model shows significantly higher gas temperatures close to the pin when humidity is increased from 0 to 15 $g.m^{-3}$ at 300 K. This water enhanced fast heating is observed from the first 200 ns after the inception of the discharge (voltage rise and pulse duration are respectively ~50 ns and ~1 µs). When the gas temperature is higher, it is demonstrated that water cluster ions decompose more easily, which increases the release of free electrons and the conductivity in the streamer plasma channel [38, 39]. If the fast heating due to humidity content arises during propagation, it may affect the discharge development. Similar effects are obtained when high electric fields are applied, which can substantially increase the ion temperature over the gas temperature [40, 41] and facilitate the de-clustering process. In the kinetic model proposed by [42], ion-molecule reactions are considered as the main mechanism of fast heating for electric fields higher than 400 Td. However, water cluster ions are not considered in this study and the effect of humidity at high electric field could not be addressed. In a similar approach [43], Aleksandrov *et al.* simulated the fast heating process in air at 1000 Td and showed that 1% of humidity (7 $g.m^{-3}$ at 300 K, about 30% of relative humidity) could increase the fraction of electron power transferred into gas heating by only 5%. Higher levels of humidity have not been tested.

In this work, focus is made on the effects of humidity on the dynamics and fast heating of a pin-to-plane high electric field diffuse discharge in air at atmospheric pressure. Section 2 describes the experimental setup and the operating conditions of discharge generation. Section 3 presents the optical methods used to determine the discharge propagation speed and the light intensity emission profiles on the pin-to-plane axis, as well as the time evolution of the gas temperature at different locations in the discharge gap. The hypothesis allowing for the consideration of the rotational temperature of excited molecular nitrogen $N_2(C)$ as the gas temperature is discussed. In section 4, results are presented and discussed according to water vapor contents and voltage amplitudes. The determination of the axial and radial temperature profiles of the discharge and the measurement of the total consumed electrical energy at the end of the applied voltage pulse are helpful to discuss the portion of energy transferred in fast heating processes. Section 5 discusses the formation and effects of water clusters on the discharge dynamic and temperature and the dependence upon high field conditions.

2. Experimental setup and electrical measurements

The diffuse nanosecond discharge is generated in a pin-to-plane configuration of electrodes being separated by a gap of 19 mm as shown in figure 1. A complete description of the device is presented in [4]. The pin is made of titanium with a 100 µm curvature radius. The plane is a copper plate (5 cm diameter) connected to the ground. Positive high voltage nanosecond pulses are generated by a FID-type technology power supply and applied to the pin. The voltage rise time is 2 ns and its width (defined from its FWHM) is about 5 ns. Each experiment is done for three maximum voltage amplitudes: 65 kV, 75 kV and 85 kV. The repetition frequency of the applied voltage is 5 Hz. The electrodes are placed in a reactor designed for controlled atmosphere and

synthetic air is flown at 1 L.min^{-1} in the direction of the pin-to-plane axis. Water vapor can be added into the air flow, upstream of the reactor, passing through a controlled temperature water evaporator and a dilution system in order to reach desired relative humidity (RH) levels from 0 to 72% (± 3%). RH is measured inside the reactor with a standard Testo 635 hygrometer. To reach high concentrations of water vapor without any condensation effects on cold spots of the gas line, two precautions have been taken: first, it has been ensured that the evaporator, placed in a temperature-controlled bath, was at least 5 °C below the ambient temperature (26.5 °C at the time of the experiment). Second, the air flow saturated with water vapor at the exit of the evaporator has been diluted with dry air just after the exit. Under those conditions of experiment, the 72% maximum relative humidity was equivalent to a water vapor concentration of 18 g.m^{-3} (2.5% of the total volume).

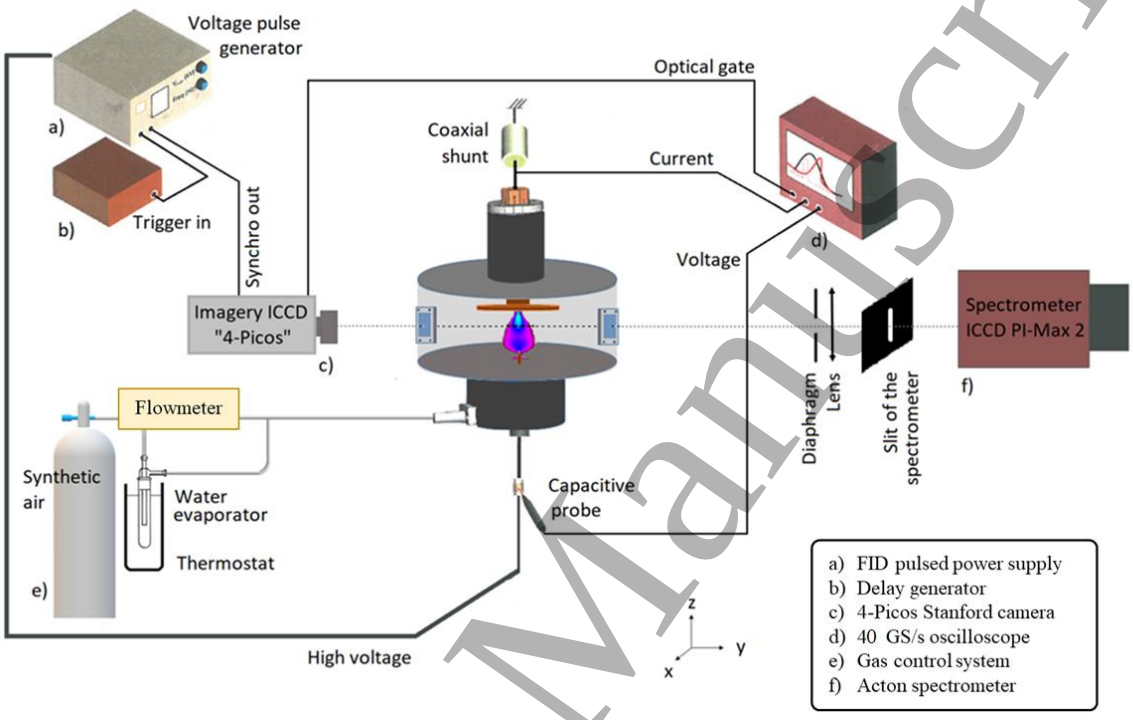

Figure 1. Experimental setup and discharge imaging with false colors

The mean electrical energy consumed by the discharge is obtained by integrating the product of the current and the voltage over the discharge duration. The voltage is measured via a home-made capacitive probe **[44]** with a bandwidth high enough to record subnanosecond signals. The current is measured with a low inductive 1.2 GHz bandwidth resistor of 0.2 Ω (TM Research Products, model SBNC-5-2) inserted between the plane and the ground. Electrical signals are recorded and processed with a sampling frequency of 40 GS/s on a 4 GHz Lecroy oscilloscope (640ZI). Typical single shot electrical signals are plotted in figure 2. In order to get an accurate derivation of the energy over such short time scale, current and voltage signals must be perfectly synchronized in time. This synchronization has been obtained by considering the capacitive current measured without discharge and fitted with the derivative of the voltage pulse. With this method, the accuracy on the mean energy is estimated to ±1.5mJ.

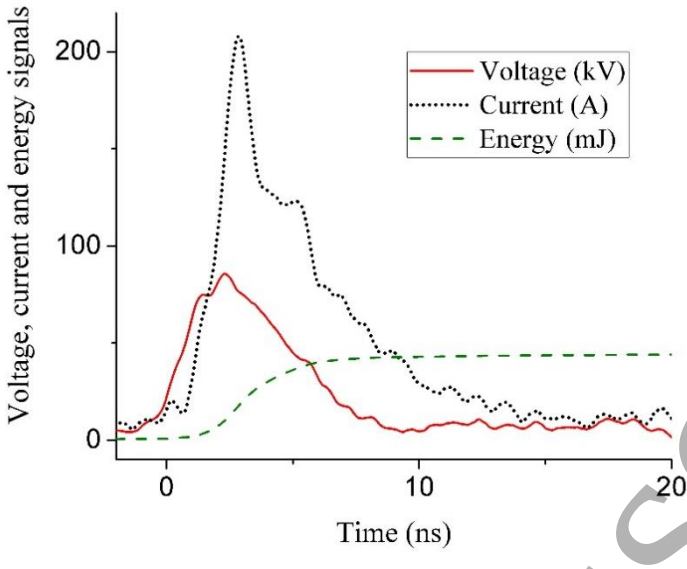

Figure 2. Single shot voltage, current and energy profiles for a typical voltage pulse of 85 kV. The origin of the time scale is chosen to coincide with the time when light emission starts to be detected at the pin.

3. Optical diagnostics

a. Light emission and propagation speed determination using subnanosecond time scale imaging

To get the time evolution of the light emission from which the propagation speed of the discharge is derived, subnanosecond time resolved imaging using a 4-Picos Stanford ICCD camera was performed. The camera is coupled to a 100 mm focal length lens system dedicated to UV light and adjusted with F/8 aperture in order to get a depth of field of about 32 mm. The light is spectrally integrated over the UV-visible spectral range, and integrated spatially over the line of sight of the camera. All sequences of images have been recorded with a time step of 100 or 300 ps and with a 200 ps exposure time gate. The time jitter is estimated to about 300 ps **[4]**. Each image has been averaged over 20 discharges. To get the speed of propagation, the position of the front of the discharge has to be defined for each image. Since the images are integrated along the line of sight of the camera, we ideally need to reconstruct the emission on the axial plane of the discharge using Abel inversion algorithm. However, as the front is located at the very tip of the discharge where light integration is done along a very short distance, the Abel inversion appears in fact not necessary. Therefore, the Abel inversion was not used for this purpose and was only used to characterize the light emission profiles on the pin-to-plane axis as shown in the next section. To define the precise location of the discharge front on the central axis, a reference absolute intensity threshold criterion has been chosen and set to about 3% of the 14-bit dynamic range of the camera. This threshold proved to be the lowest value giving a clear definition of the discharge front in any conditions (instant of propagation and working condition). This intensity threshold has been kept the same for all experimental conditions. The propagation speed uncertainties presented in the following graphs are obtained using a linear regression method. They range between ± 0.07 $mm.ns^{-1}$ and ± 0.3 $mm.ns^{-1}$ depending on the speed range. They are similar to the experimental uncertainties estimated by repeatability measurements, which range between ± 0.1 $mm.ns^{-1}$ and ± 0.3 $mm.ns^{-1}$.

b. Light spectral analysis using spatially resolved Optical Emission Spectroscopy

To determine the gas temperature during the discharge, Optical Emission Spectroscopic (OES) experiments have been conducted. The light emitted from the discharge mainly originates from the Second Positive System of molecular nitrogen (N_2(C-B)). It has been recorded and analyzed using a 75 cm focal length imaging spectrometer (Acton SP 2750 PI) equipped with a PI-MAX 2 ICCD camera. The time gate resolution can be set to be as low as

500 ps. A 2400 lines.mm^{-1} grating has been mainly used to achieve a maximum spectral resolution of down to 0.04 nm. Two setups have been used. To obtain spatially integrated spectra, a UV optical fiber (SR200, diameter: 0.72 mm, numerical aperture: 0.22) has been set directly in front of a quartz window to collect the total light emitted by the discharge during the whole voltage pulse. To get spatially and temporally resolved measurements, the light has been collected by a 20 cm focal length UV lens focused on the entrance slit of the spectrometer. A diaphragm of 3 mm radius has been set in front of the lens in order to limit the solid angle of collection to 3.10^{-4} sr. With this setup, only the light coming almost perpendicularly from the pin-to-plane axis is collected through the slit, so that light spatial integration along the pin-to-plane axis is strongly reduced. Considering the whole optical system and referring to the spatial coordinate indicated in figure 1, the resolution along the z-direction is estimated to be better than 150 µm. This value is low enough to correctly describe high temperature gradients in the pin region, while the amount of the collected light still guarantees a high signal-to-noise ratio of the recorded spectra. The width of the entrance slit of the spectrometer is about 100 µm and it is set parallel to the pin-to-plane axis. With this configuration, each single acquisition contains the spectra for all positions along the z-axis. As the time evolution of the temperature is rather slow, light could be reasonably integrated over 3 ns to improve the signal-to-noise ratio of the recorded spectra.

Since the discharge is about 2 cm large (in the x and y directions) and inhomogeneous, the Abel inversion of the spectra is required. As the slit is aligned along the z-axis, spectra along the x-direction are captured by translating the lens along with the diaphragm with a spatial step of 300 µm. As each measure is integrated over 6000 discharge events, the number of spectra that can be recorded along the x-direction for a single profile is limited. In general, 25 spectra are recorded per profile to describe the integrated axial evolution at a given position along the z-direction. To reconstruct the radial evolution of the spectra, the Abel inversion has to be done wavelength by wavelength. First, the axial profile of each wavelength is reconstructed. This profile is carefully fitted with a gaussian function to interpolate the data over the 300 µm between each step, then it is Abel inverted with the method from **[45]**. The choice of the fitting function has no physical meaning, it is only meant to describe the axial profile as well as possible. Finally, radial profiles are placed end to end to build the complete inverted spectra of each radial position.

As it is usually done in the literature for different types of atmospheric pressure non-equilibrium plasmas, the gas temperature is considered to be equivalent to the rotational temperature of $N_2(C)$ excited state of molecular nitrogen. The latter temperature can be derived from the comparison of the high-resolution experimental and synthetic ro-vibrational spectra of the $N_2(C\text{-}B)$ transition (Second Positive System – SPS). In this work, the $N_2(C)$ rotational temperature is mostly determined by comparing the experimentally recorded emission of the (0,0) ro-vibrational band of $N_2(SPS)$, which has its peak intensity at 337.13 nm, and the corresponding synthetic spectra which are generated either by the fitting code given in **[46, 47]** or by the code from **[48, 49]**. Figure 3 shows an example of a fitted experimental spectrum of $N_2(C\text{-}B)$ (0-0) emission and the corresponding gas temperature. The (0-1) transition at 357.69 nm has been also used in some representative cases for verification and estimation of measurements accuracy.

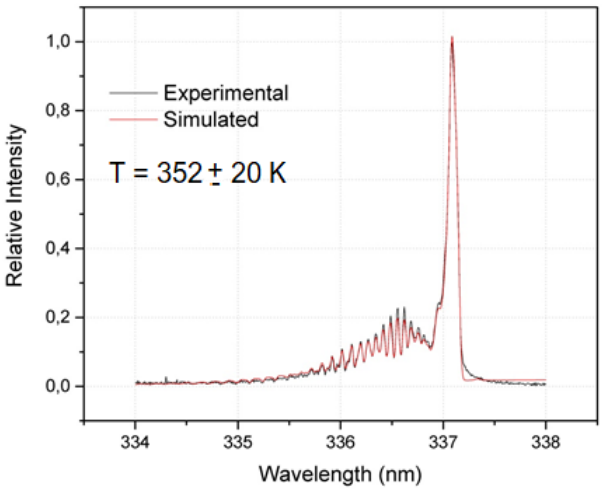

Figure 3. Typical experimental and simulated rotational spectrum of the N_2(C-B) (0-0) transition.

c. Validity of the gas temperature determination from the rotational temperature of N_2(C)

To ensure the equivalence between the N_2(C) rotational temperature and the gas temperature, we cannot consider that the rotational-translational relaxation is fast enough to achieve a thermal equilibrium of N_2(C) molecules before their radiative de-excitation. Indeed, the commonly used assumption that the rotational relaxation time of N_2(C) is very small compared to its lifetime is not satisfied under our conditions. The lifetime of N_2(C) can be determined considering the main three reactions of depopulation of the N_2(C) state and their respective characteristic frequency given in table 1 (at 300 K). Each frequency is given by the inverse of the characteristic time given in the table. The equivalent lifetime of N_2(C), given by $\tau_C = 1/(\nu_1+\nu_2+\nu_3)$, is about 0.7 ns under our discharge conditions, which is very close to the rotational-translational relaxation time of about 0.4 ns [50], thus preventing a safe conclusion on the thermalization of N_2(C).

Table 1. Main N_2(C) loss reactions and reaction rate constants at 300K

Reaction	Reaction constant	Characteristic time (ns)	*Reference*
$N_2(C) \rightarrow N_2(B) + h\nu$ (1)	$2.8\ 10^7\ s^{-1}$	36	*[51]*
$N_2(C) + N_2(X) \rightarrow N_2(a') + N_2(X)$ (2)	$10^{-11}\ cm^3.s^{-1}$	5.2	*[52]*
$N_2(C) + O_2 \rightarrow N_2(X) + O + O$ (3)	$3\ 10^{-10}\ cm^3.s^{-1}$	0.69	*[52]*

However, as suggested in [53], the main specificity of the discharge studied here is the extremely high electric fields generated [22], which are sufficiently high for N_2(C) to be created mainly by direct electron impact: $N_2(X) + e \rightarrow N_2(C) + e$. Yet, it is demonstrated that the creation of excited states through direct electron impact implies that the rotational population distributions ($P(J)$) of molecules in the fundamental and excited states are identical and, for a given molecule, the quantum rotational number J is preserved [54] Therefore, the rotational distribution in the N_2(C) state, $P_{N2(C)}(J)$, is equal to the rotational distribution in the ground state, $P_{N2(X)}(J)$, and, because their rotational constants ($B_{N2(C)}$ and $B_{N2(X)}$, respectively) are different, the equality of those rotational population distributions implies a difference in their mean energy. Considering Boltzmann distributions: $P(J) \propto S(J)(2J+1)e^{-\beta_i B_i J(J+1)}$ where $S(J)$ is the nuclear spin, B_i is the rotational constant of the species i and $\beta_i = \frac{hc}{kT_i}$ is the energy. The equality of the rotational distributions entails different rotational temperatures between N_2(C) and N_2(X) when N_2(C) is created by electronic excitation. Therefore, the possibility of using OES to get the gas

temperature during the discharge requires a quantification of the temperature discrepancy due to the difference between the rotational constants of both states. However, these rotational constants are very close and the difference between the rotational temperatures of $N_2(X)$ and $N_2(C)$ just after impact is therefore relatively small. To simplify, the energy model has been restricted to the case of the rigid rotator, valid for small J. Indeed, the resolution of the optical spectrometer allows to solve at most fifteen rotational lines for the vibrational transition $N_2(C, v' = 0) \rightarrow N_2(B, v'' = 0)$, and the error made with respect to the centrifugal distortion approximation, which increases at J^4, remains less than 0.1% up to J=15.

It is well known that by plotting the logarithm of $\frac{P(J)}{S(J)(2J+1)}$ as a function of the rotational energy, points align according to the rotational temperature. It is therefore possible to estimate the maximum temperature difference for a fixed temperature of the ground state $N_2(X)$ simply by calculating the ratio: $T_{N2(C)} = \frac{B_{N2(C)}}{B_{N2(X)}} T_{N2(X)}$. With $B_{N2(X)} = 1.98959$ cm^{-1} and $B_{N2(C)} = 1.81742$ cm^{-1} (NIST database), it follows that the gas temperature obtained by OES from the N_2(C-B)(0-0) transition is then underestimated by 28 K for $T_{N2(X)}$ = 330 K. At 750 K (which is the maximum temperature observed at the pin by OES), the temperature is underestimated by 65 K. However, this estimation cannot be used as a correction factor since some $N_2(C)$ molecules will undertake one or few collisions before they relax on $N_2(B)$ state by radiation. Therefore, the population distribution of these $N_2(C)$ molecules would have changed and the rotational temperature of $N_2(C)$ would be closer to the rotational temperature of $N_2(X)$. Consequently, the bias of 28 K and 65 K are just upper limits, important to keep in mind. They will not be considered in the results below.

Last, as stated previously, the rotational-translational relaxation of $N_2(X)$ is about 0.4 ns for our experimental conditions and it can be considered faster than the temporal evolution of the temperature during the discharge. We can consider that the thermal equilibrium of $N_2(X)$ is reached while it is excited to $N_2(C)$ states and that the rotational temperature of $N_2(C)$ can be finally considered as representative of the gas temperature. This last assumption could only be questionable at the highest applied voltages for positions near the pin electrode, where the temperature rises with a rate of about 100 K.ns^{-1} at the end of the voltage pulse.

4. Experimental results

a. Threshold effect on the reduction of the propagation speed with increasing humidity

Figure 4 a) shows the integrated UV-visible emission of the discharge just after the junction of the discharge at the plane (1.6 ns), at 85 kV, in air at RH<2% and for a gap of 18 mm. The discharge is diffuse and covers a volume of about 1.5 cm^3 in these conditions. The addition of water vapor does not destabilize the high electric field discharge which remains stable and diffuse. The evolution in time of the discharge front position along the pin-to-plane axis is given at 65 and 85 kV in figure 4 b. For each voltage, the front positions are shown at RH<2% and at RH=72%. These conditions reflect the most different conditions studied and are used hereafter to determine a unique experimental procedure that determines the discharge propagation speed for any condition. The inception of the discharge is chosen to coincide with the time when light emission is detected at the pin, while the end of the propagation coincides with the time when the discharge reaches the plane. Whatever the experimental conditions, the discharge front extends linearly over most of the gap distance, until the discharge approaches by less than 5 mm from the plane. This is represented by the grey section in figure 4 b. The propagation speed of the discharge can be determined using a linear regression method over this length range and it can be considered constant. The propagation speed values presented hereinafter are derived over this length range. When the discharge gets close to the plane, the propagation accelerates dramatically. Also, the common observation can be made that propagation is faster as voltage increases.

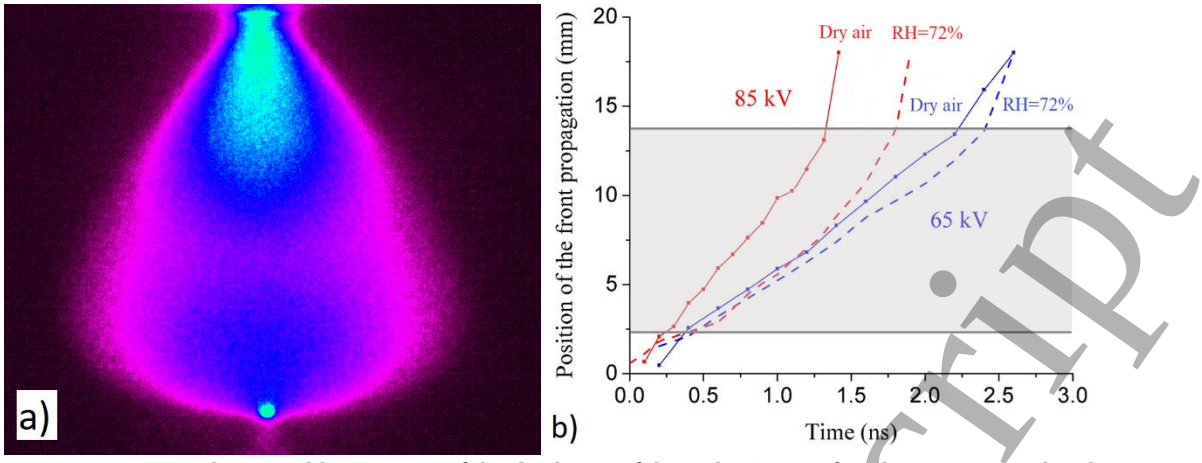

Figure 4. a) Integrated UV-visible emission of the discharge (false colors) just after the junction at the plane (1.6 ns), at 85 kV, in air at RH<2% and for a gap of 18 mm. The pin is at the bottom and the plane at the top b) Position in time of the discharge front at 65 kV (blue) and 85 kV (red) and two different gas mixtures for a gap of 18 mm. RH<2% (solid line + scatter) and unsaturated air-water mixture at RH=72% (dashed lines). The length range in the gap where the discharge propagation is linear and from which the discharge propagation speed is determined is shown in grey and is valid for any condition.

For a better representation, figure 5 depicts the discharge propagation speed versus the voltage amplitude in dry and humid air. Each speed value is an average of 2-5 records such as those presented in figure 4. The increase of the speed uncertainty with the voltage is due to the experimental method used. The same 100 ps time step between each image has been set within a discharge sequence, while the whole propagation time decreases at higher voltages. Therefore, fewer measurements along the gap were accounted for the linear regression. At high voltages, above 75 kV, the experimental results reveal the existence of a threshold of relative humidity, around 30%, above which the propagation speed is significantly lowered. A significant drop of about 30% of the speed is observed for any relative humidity above 30%. For the lowest voltage amplitude, the effect is smaller (10%). As discussed in section 5, this behavior suggests either the occurrence of a new mechanism directly related to high water vapor contents, or the modification by water vapor of a mechanism already existing in dry air, both strongly enhanced in high electric field conditions.

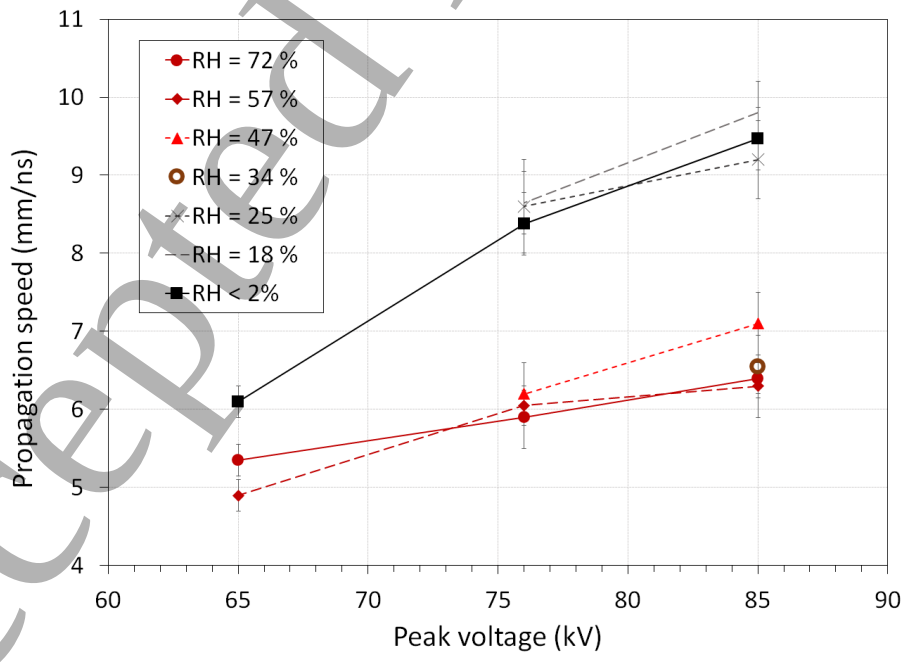

Figure 5. Propagation speed of the discharge for three different voltages (65, 75, 85 kV) in dry air (solid black line) and unsaturated air-water vapor mixtures at different RH.

b. Enhancement of light emission intensity at the pin with humidity

The discharge dynamics and its reactivity significantly depend on how the electrons and the electric field are both simultaneously distributed in space and time. Related to the expression of the electric power density, $j.E$, the locations in the discharge for which both the electric current density j (associated to the electron density) and the electric field E are high enough will be subjected to enhanced collision rates and chemical reactivity. Therefore, the light emitted in the discharge gap (resulting from de-excitations after electronic impacts) reveals the regions where these conditions are fulfilled. As a reference, in a low-voltage positive streamer discharge, it is primarily the head of the discharge where both field and electron density are high that emits light. At the front of the streamer head, the electric field is high, but the electrons are few. At the back of the streamer head, inside the plasma channel, there are many electrons, but the field is too low. In the high electric field discharge studied here, the situation is much different, and the field is still high enough at the front and at the back of the high field region to produce light revealing a significant plasma activity **[18, 21, 22]**. According to those considerations, the following section provides interesting results on the effect of humidity on the spatial distribution of the discharge emission.

With the same fast imaging data as those in the previous section, the wavelength-integrated light emission profiles at the pin-to-plane symmetry axis, integrated along the line of sight of the camera, have been analyzed and processed by Abel inversion. Figure 6 compares profiles in at 85 kV at 1.5 ns after the inception of the discharge for RH<2%, RH=25%, RH=34% and RH=72%. The pin is located at 0 mm on the pin-to-plane axis and the plane is at 19mm. Light is more intense at the pin because of the higher electric field amplitudes and then it decreases monotonously towards the plane. There are significant changes of light intensity profiles with increasing relative humidity. First, emission is more intense close to the pin at high relative humidity levels. At 1.5 ns after the discharge inception, emission stays close to 0.4 (a.u.) for dry air and relative humidity lower than 30%, but it is twice higher for relative humidity values higher than 30%. This discrepancy is hardly visible in the early stage of the discharge and starts to appear at about 0.6 ns, which corresponds to a voltage amplitude of 48 kV. Second, as shown in figure 7, the light emission at the pin decreases faster in highly humid air than in dry air and it is less intense in the rest of the gap.

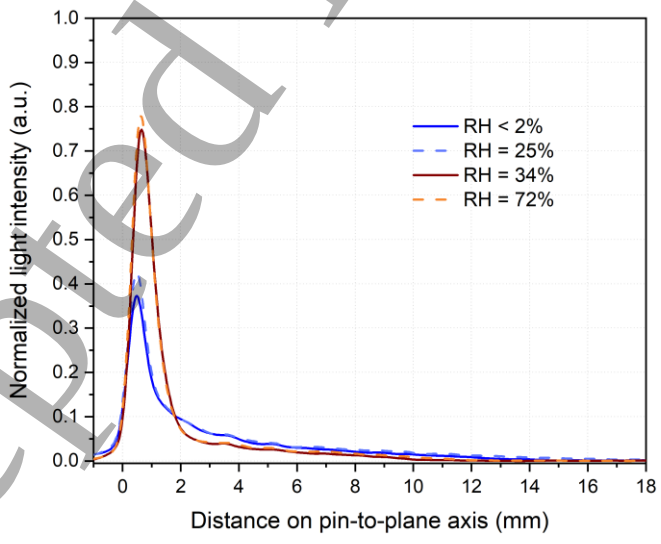

Figure 6. Comparison of wavelength-integrated light intensity profiles at 85 kV, 1.5 ns after the start of the discharge, for RH < 2%, RH=25%, RH=34% and RH=72%.

There is a strong correlation between light emission intensity and the discharge propagation speed dependences with relative humidity. Those changes in the light intensity distribution are also submitted to the threshold effect around 30% of RH, as shown in figure 7. The light intensity is plotted at 65, 75 and 85 kV, at the pin location and

at 3 mm away from it, when the discharge has reached the plane. The position at 3 mm represents the distance from the pin where the reduction of the light intensity, just above the peaked pin region, is the most pronounced. For the two highest voltage amplitudes, the evolution with RH of light intensity at the pin is characterized by a break at a threshold around 30%. To a much lower extent, the light intensity at 3 mm from the pin is subjected to a faint decrease at the same threshold, which however is found to be within the measured error bars. Both the propagation speed and the light emission intensity are modified by the water vapor content in air only at very high applied voltages. The responsible mechanism that explains this threshold effect is related to very high electric field conditions. Possible responsible mechanisms are discussed in section 5.

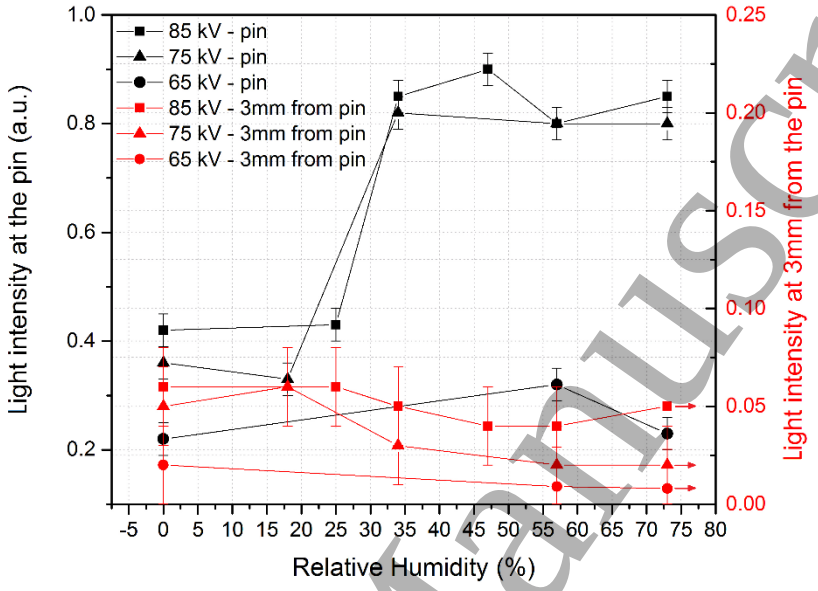

Figure 7. Evolution with RH of the light intensity at the pin (in black) and 3 mm away from the pin (in red) at 65, 75 and 85 kV.

The intensification of light emission with humidity around the pin and the deceleration of the discharge as soon as it starts from the pin could be correlated to a modification of the gas temperature in the same region. The processes for which the rate constants are temperature dependent could be strongly affected. The next section is dedicated to the determination of the gas temperature by OES and to the comparison of the spatially resolved measurements in dry and humid air.

c. Discharge total energy and gas temperature under dry and humid air conditions

The variation of the mean electrical energy (see section 2) consumed by the discharge versus the RH during a single voltage pulse is presented in figure 8. In dry air, at 65 kV, the mean energy is about 12 mJ. At 75 kV, it reaches 32 mJ and increases further to 62 mJ at 85 kV. We observe that the mean energy is slightly lower when water vapor is added almost independently of its concentration. This energy drop is stronger at higher voltages (about 8 mJ at 85 kV) and noticeably lower at 65 kV (only 2 mJ) corresponding to about the same relative decrease of 17%. This drop on the mean discharge energy is in good agreement with the slowdown of the discharge propagation when water is added at the highest concentrations, as discussed in section 5 d.

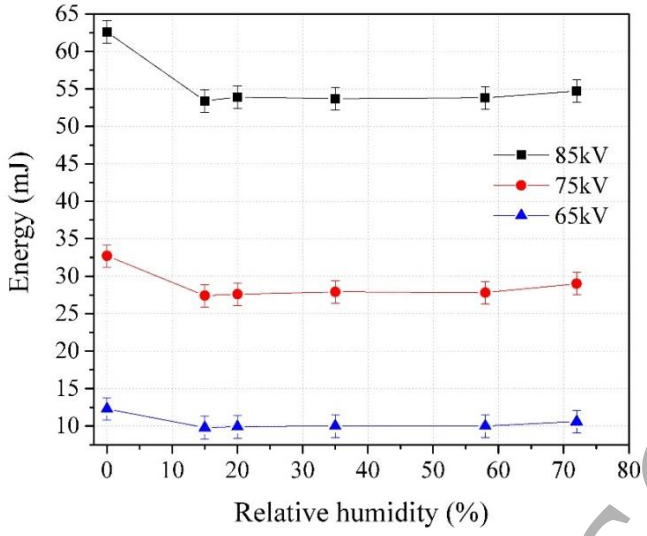

Figure 8. Electrical energy consumed by the discharge for different water vapor contents at 65, 75 and 85 kV. Error bars come from the dispersion of measured energies over a series of experiments.

Even if the energy consumed by the discharge within only l0 ns is rather high, with a maximum current intensity as high as 200 A, the average gas temperature remains low, close to 330 ± 20 K at 85 kV, independently of the concentration of water vapor. Figure 9 illustrates average gas temperature measurements integrated over the whole discharge volume and over time (10 ns). They were obtained with the first setup as described in section 3b. The estimated error from the fitting is ± 20 K at 75 and 85 kV where the signal-to-noise ratio (S/N) is high and between +40 K and -20 K at 65 kV, where the S/N ratio is low and temperature values below 290 K are unrealistic. Despite the uncertainty on these measurements, a slight increase of the temperature with the voltage can be observed.

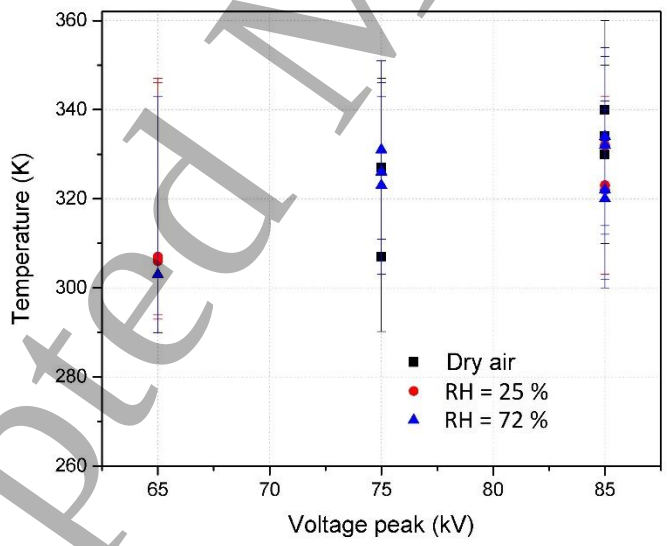

Figure 9. Average gas temperature integrated over time (10 ns) and space (entire gap) in dry and humid air (25 and 72% RH), at 65, 75 and 85 kV.

It should be noted that temperature measurements averaged over the whole discharge volume hide its local variations. Figure 10 shows spatially and temporally resolved temperature measurements in dry and humid air, at 85 kV, for three specific locations on the pin-to-plane axis: just at the tip of the pin, at the middle of the gap and close to the plane. These data have been obtained with the second setup described in section 3b. The temperature in highly humid air (72% RH) has been determined only at 9.5 ns after the start of the discharge, as

will be explained in the following paragraph, when heating is significant. It appears that the temperature profiles are highly inhomogeneous. Heating is almost concentrated at the pin where 650 ± 90 K are reached at 9 ns in dry air. The central area of the discharge stays very close to the room temperature with an increase limited to about 20 ± 10 K. At the plane, where a constriction of the plasma and an increase of the light emission are observed, the temperature increases of about 40 ± 10 K. For high humidity levels, as the light is more intense at the pin, it is not surprising to observe a slight increase of the gas temperature. It is also clear that, both in dry and humid air, the gas temperature increases significantly at the pin in a very short time period and fast heating mechanisms as those described in [42] are at stake. However, it starts only after the discharge propagation and junction to the plane at 1.5 ns. Before this very short time period of propagation, those mechanisms are not efficient enough or do not apply and gas heating remains negligible. At 65 kV, a similar behavior is observed but the temperature rise is much weaker, it has only reached 365 ± 10 K at the pin at 9 ns.

In order to make a meaningful comparison of heating in humid and dry air conditions at 85 kV, we have to consider that the discharge propagates slower in humid air and reaches the plane 0.5 ns later within the voltage pulse, as shown in figure 4. The same time period right from the plane junction must be considered for both conditions, which means that the gas temperature at 9 ns in dry air must be compared to the temperature at 9.5 ns in humid air. Therefore, an increase of about 100 K is observed near the pin at the highest humidity level. This effect is significant and reproducible, though within error margins. Since this increase is not observed anywhere else in the gap, it supports the idea that humidity effects are correlated to the specific high field conditions studied herein.

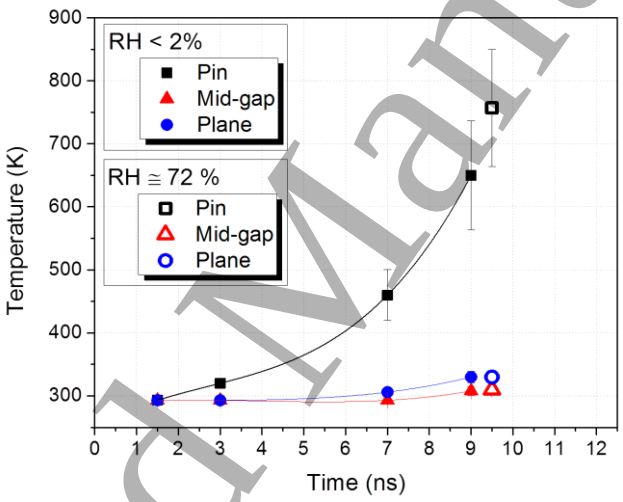

Figure 10. Time evolution of the gas temperature in dry and humid air (72% RH) at 85 kV. Three locations along the gap (pin, mid-gap and plane) are investigated. Time resolution is 3 ns. Time origin corresponds to the start of the discharge at the pin.

A complete 2D mapping of the gas temperature at 9.5 ns, 85 kV and 72% of relative humidity is given in figure 11. This mapping can be used to determine the amount of energy spent in fast heating. Using the cylindrical symmetry of the discharge, the sensible heat C_{air}*ΔT is determined in the whole discharge volume. C_{air} is the temperature-dependent heat capacity of air and ΔT is the difference between gas temperature and ambient temperature. In order to calculate the heat, the total discharge volume (about 1.5 cm^3) has been discretized in elementary volumes of about 3.10^{-2} mm^3 each, in which temperature is supposed to be uniform. Given the uncertainties of the measurements and the sensitivity of sensible heat calculations to temperature variations, the method only provides an order of magnitude of the energy spent in fast heating. In dry air at 85 kV, the temperature measured by OES at the end of the voltage pulse suggests that about 10 mJ is spent in fast heating. It represents about 16% of the electrical energy injected in the gap. In humid air, it is about 18%, which is very similar. However, the energy is not distributed alike. If we look at the temperature distribution separately within delimited areas of the discharge, the energy spent in heating at the pin is higher in humid air than in dry air, which is not the case near the plane. In a region axially limited to 3 mm away from the pin but unlimited in the radial direction,

heating represents 1.0 ± 0.4 mJ at 9ns in dry air, and reaches 2.1 ± 0.4 mJ at 9.5 ns for RH=72%. For these identical two times, the energy spent in the region axially limited to 4.4 mm away from the plane is nearly the same in dry and humid air and is about 4 ± 1 mJ. In the middle of the gap, the temperature increase is so weak that the choice of the volume on which the heat should be determined is not accurate. The accuracy at the pin is much higher since heating is clearly delimited in space.

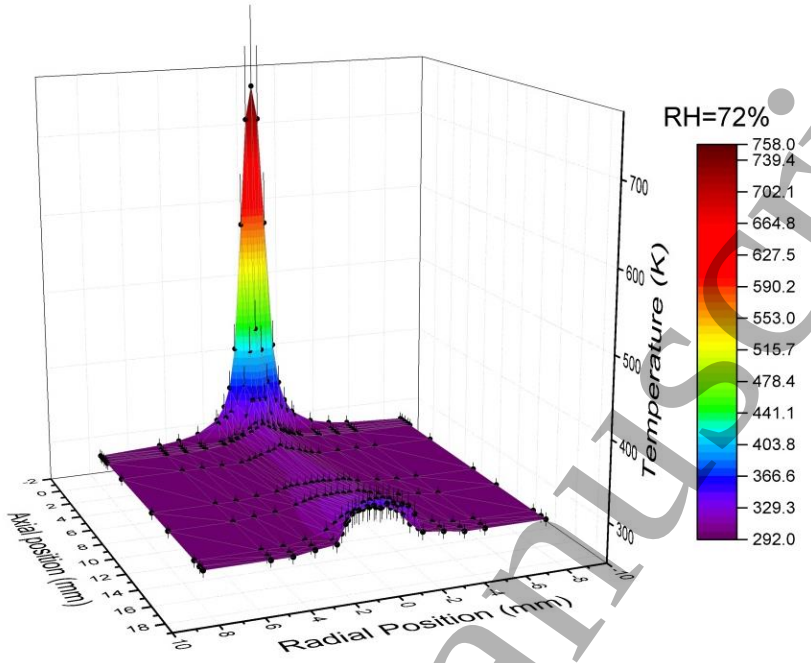

Figure 11. Gas temperature 2D profile in humid air (72% of RH) at 85 kV. The profile is determined at 9.5 ns after the start of the discharge. Thin black segments represent the uncertainties from the fitting method.

Those results show that the water vapor addition can enhance the heating processes in a few nanoseconds in the high field region of the pin but not in the areas where the field is lower. The gas temperature during the early post-discharge has been also obtained by spontaneous Raman scattering [55]. Those measurements showed that the temperature spatial mapping in the first 300 ns of the post-discharge suggests that 1 ± 0.4 mJ is spent in fast heating at the pin in dry air and 1.5 ± 0.4 mJ in humid air. These results are completely coherent with the OES results presented in this work. Another important result which is confirmed by those Raman scattering measurements is the existence of the same humidity threshold on gas heating with a temperature increase of 200 K only above 30% of relative humidity. Those results will be detailed in a future publication.

5. Discussion

The discussion section is devoted to the mentioning of various process that could explain the aforementioned observed mechanisms. The study of these hypothesis should be tackled in future experimental and modelling works.

a. On the formation of water clusters at high humidity levels

The results on the effects of the relative humidity on the propagation speed and light emission of the discharge prompts to focus on the interaction of electrons and photons with water. Those interactions have been studied for decades; however, it is still a modern field of research. One difficulty is that they show substantial disparities whether they relate to isolated water molecules [56-57], small clusters [58-59], aerosols or even micrometric droplets. For instance, the electronic affinity of an isolated water molecule being almost zero, it will hardly capture electrons. However, a small cluster of two molecules is enough to capture electrons and the binding energy

increases with the size of the clusters with different binding states observed from surface states to solvated electrons [58]. Similarly, the absorption spectrum of UV light in the range of photons emitted by nitrogen that lead to photo-ionization of O_2 (~100 nm), is strongly dependent on the state of water: isolated water molecules show little absorption in this range [57, 60] while liquid water and probably large clusters and droplets in condensed phase show very strong absorption coefficients of about 10^8 m^{-1} [61].

In our experiments, the 30% humidity threshold effect observed on the propagation speed and light profiles (see figures 6 and 9) suggests the presence of water clusters that would appear only at the highest humidity conditions. A work from Tsuchiya [62], which measured the size distribution of water clusters by liquid mass spectrometry in air for various humidity contents, could support this observation. It was shown that a transition occurred above 30% humidity. At low relative humidity, the mass spectrum of water clusters revealed two distributions, one of small clusters made up from 2 to 8 water molecules, and a second one of bigger clusters from 9 to 24 molecules. As the degree of humidity increases, the proportion of these two distributions progressively shifted from the one of small clusters to that of large clusters. The presence of the distribution of small clusters was explained by the detachment from clusters of more than 25 molecules of a small cluster of 4 to 7 molecules by dilution in air. Conversely, when the degree of humidity is higher than 30%, the cluster size is not limited anymore to 24 molecules. The distribution shows a single envelope, the maximum abundance of which increases progressively with the degree of humidity. Thus, a change of the interaction of electrons and photons is expected as the properties of water clusters change significantly above 30% humidity.

Two other processes can be mentioned, albeit very unlikely because they develop in much longer time scales than the time scale of the discharge propagation. The first process is the formation of large water aggregates through coagulation or condensation on nuclei present in the gas. The modification of the distribution of water cluster by introducing some impurities to the gas is known for pin-to-plane or dielectric barrier discharges. These impurities can come from a smooth but significant erosion of the electrodes, enough to produce metallic vapors on which physical nucleation occurs [63-64]. Through coagulation or condensation processes, those nuclei grow and form into large size water aggregates. Mean radii larger than 50 nm are expected as Mie scattering has been qualitatively observed during LIF experiments made with high water content in similar discharge conditions. The time scale of water aggregates formation is, however, longer than that of the discharge propagation. In addition, considering the very low pulse repetition rate of 5 Hz and the air flow of 1 $L.min^{-1}$, those aggregates could be carried away from the vicinity of the pin from one discharge to another and can barely have an effect on the discharge inception. The second possible process of water aerosol formation is related to water condensation directly at the surface of the electrodes. Particularly at the pin, at high levels of humidity and stressed by high electric fields, a thin liquid film formed at the surface could induce a Taylor cone and spray into water aerosol in the gap [65]. However, the discharge dynamics is shorter than a few nanoseconds and such an electro-hydrodynamic process is not possible within this time scale. Therefore, both aforementioned processes are unlikely to affect the discharge dynamics.

b. Effects of water clusters on the discharge dynamics

Water clusters have certainly no effect on the very start of the discharge, but they can influence its dynamics as soon as it propagates towards the plane. Simulation of electronic transport coefficients (mobility, drift and diffusion) with the BOLSIG+ solver [66] in humid air shows no significant modification in the field range of 100 to several thousands of Townsend. As mentioned in the introduction, the electron attachment increases significantly in humid air, but it remains negligible compared to the ionization coefficient at fields higher than 100 Td. Then, the effective ionization coefficient is almost independent from humidity. Notice that BOLSIG+ considers water as isolated molecules and does not simulate water clusters which have specific coefficients. Interesting data on electronic attachment and photon absorption by water aggregates can be found in the literature [34, 58, 61]. High attachment cross section on water clusters at electronic energies close to zero and higher UV photon absorption with very large clusters, could both impact the propagation of the discharge and the spatial distribution of light emission. As considered in streamer-leader propagation in long air gaps [25], the increase of the electron attachment in the bulk of the plasma created behind the discharge front reduces its conductivity and attenuates the space charge field in the front. It makes the propagation globally slower and the field becomes

higher at the anode and induces a stronger emission intensity. Higher fields in the pin region could also explain the increase of gas heating at highest humidity levels (see figure 11) when ions, and particularly water cluster ions, are considered to be the main source of fast heating [42]. The efficient absorption of 100 nm range photons by large water aggregates may also participate to the slowdown of the discharge. Auto-absorption of photons, mainly emitted around 337 nm, cannot be considered at high humidity to explain the decrease of the intensity from 2 mm away from the pin (see figure 7) as absorption coefficient is about 10^{-1} m^{-1} at this wavelength.

c. Dependence upon high field conditions

The effects observed on the discharge cannot be attributed only to the formation of large water clusters at high humidity levels. The main point is that the threshold effect is not observed at the lowest voltage of 65 kV or it is at least very weak. The mechanisms responsible for this humidity effect are therefore electric-field dependent and they are enhanced only by very strong electric fields. The formation of aggregates from metallic nuclei resulting from electrode erosion could be one of these mechanisms since, at the highest voltage, high energy electrons can suspend larger amounts of condensation nuclei. Even just higher concentration of metallic vapors could enhance the process of water cluster size shifting described in [61] at humidity levels higher than 30%. In any case, we therefore consider that high water vapor content reveals here a specific field-structure of the discharge, different from the classical streamer concept where the field is completely screened close to the anode. As described in [22] at the highest overvoltage, a field stronger than 800 Td is maintained at the pin over 1 ns and remains higher than 300 Td over 6 ns. When the applied voltage is reduced down to 65 kV, the field at the pin decreases down to 200 Td much more rapidly. Water molecules tend to destabilize the high overvoltage regime, as observed in a previous work with a few percent of hydrocarbons [24], and bring the dynamic properties of the discharge closer to those described at lower voltage (see figure 5). The threshold humidity effect on the discharge inception for medium size gaps under DC voltage, described in [25] and recalled in the introduction, is somehow similar to our concern since it is also related to a modification of the discharge regime (streamer to glow).

What kind of high field-dependent processes could be therefore altered by water vapor or clusters? Assuming that high field diffuse discharges can definitely involve runaway electrons and X photons from their interaction with electrodes, water molecules or aggregates in the gas phase can prevent some of those electrons to accelerate up to the runaway regime and limit their mean energy. They can also absorb X radiation on shorter distances and make the self-preionization described in the introduction less efficient. Finally, water vapor condensation at the anode at high levels of humidity can affect the nature of the interaction of the electrons with the electrode and make the generation of X-rays less efficient. This last assumption could be reasonable to address the 30% threshold effect. Even if the amount of isolated water molecules remains very small compared to nitrogen and oxygen, they could be a new source of electrons as well. According to the NIST data [67], the adiabatic ionization potential of water (12.62 eV) is lower than that of nitrogen (15.58 eV) and comparable to that of oxygen (12.07 eV). Under conditions of a sufficiently high electric field, i.e. at the highest voltage of 85 kV and very close to the pin, ionization of isolated water molecules will be sufficiently efficient to increase the electron density and enhance the light emission intensity. This effect would be negligible at 65 kV as the electric field remains too low. However, how to explain the threshold effect with the humidity level? Over 30% of relative humidity, assuming the formation of clusters, they could enhance this ionization process. No experimental data are available for the ionization energy of such clusters but results of calculation ab initio can be found in the literature [68]. They show that the adiabatic ionization potential decreases with the number of water molecules in the cluster, from about 10.75 eV for the $(H_2O)_2$ dimer, to 10 eV for $(H_2O)_3$, and down to 9.3 eV for the $(H_2O)_6$ hexamer which is close to the ionization potential for liquid water. It is therefore easier to ionize clusters than single water molecules.

d. Energy, Gas heating and humidity effects

The energy dependence on humidity is probably linked to the effect of humidity on the discharge speed and inception voltage. The discharge propagates slower in the gap in presence of water vapor and reaches the plane later within the voltage pulse. It means that the plasma conduction phase is shorter in time. Since most of the energy is consumed during the conduction phase, this slowdown leads to lower amounts of consumed energy. The

measurement of a lower maximum current intensity at high relative humidity supports this explanation. This energy decrease is the same for the whole RH range, which is surprising for 15 and 20% of RH, for which the results on the light emission and speed show that there is no influence of water at the lowest concentrations and under the threshold of 30% of RH. It means that besides the influence on the propagation speed itself, the water content may have also an effect on the inception of the discharge. If water content is assumed to change the conditions of the inception of the discharge and, more specifically, the voltage threshold, one could explain why the discharge energy would be different between dry and low humidity conditions, while the speed remains the same. Unfortunately, this assumption is difficult to check since the accuracy on the inception voltage measurement is very low. Because the voltage rise rate is of about 40 kV.ns^{-1} at 85 kV, a usual time jitter of 300 ps in the experiment leads to an uncertainty of more than 10 kV on the voltage amplitude determination.

Gas heating and its dependence to humidity is also an indicator of the specificity of the discharge at the highest voltage. At 65 kV, no heating can be measured even close to the pin, the gas temperature remains close to ambient and the humidity shows no influence at all. At 85 kV, significant heating is observed within a very short time period (< 10 ns) only in the high field region near the pin and the humidity enhances the heating processes being involved. Processes such as V-T relaxation of H_2O vibrational modes described in **[37]** cannot satisfactorily explain this effect as their time constant of about 40 ns remains higher than the discharge time scale. A more likely consideration is the role of ions and the substantial increase of their kinetic energy in the high electric field maintained close to the pin over several nanoseconds at 85 kV. They can transfer efficiently a part of this energy to neutrals and in the case of water cluster ions at high humidity levels, this transfer could be reasonably higher.

Independently of humidity effects, the fraction of the discharge total energy converted into heat within the voltage pulse is estimated to a bit less than 20% at the highest voltage amplitude. During this time, the electric field is changing and, most of all, it is not uniform with much higher strengths close to the pin. In the main part of the gap, where the field remains below 200 Td **[22]**, heating is quite weak, but it concerns a large volume of gas such that the energy transfer in this low-field part of the discharge is about 14%. Near the pin, the field can increase up to 800 Td and heating is more intense but, within a much smaller area, it represents only 2% in dry air and 4% in humid air.

6. Conclusion

Based on space and time resolved OES measurements, this experimental work provides new results on the dynamics of diffuse discharges generated by high overvoltage nanosecond pulses in a pin-to-plane air gap. The focus is made on the influence of water vapor content in air on the dynamics of the growth of the discharge and fast heating processes. No influence is observed under 30% of relative humidity, i.e. 7.5 g.m^{-3} of water vapor under our conditions of pressure and temperature. Above this threshold, the speed is significantly lowered, and light emission profiles are modified with an intensification close to the pin. The discharge energy is a bit lower with water vapor almost independently of its concentration. In humid air, fast gas heating is significantly increased only in the pin region and it reaches about 18% of the total energy of the discharge. However, all these effects concern only the highest voltage amplitude of 85 kV. At the lower voltage of 65 kV, the speed, the light profile, and the gas temperature are not affected by the water content. The differences between those two voltage conditions definitely show that diffuse discharges generated under very high overvoltage exhibit their unique features, particularly concerning the electric field dynamics.

The most likely interpretation that we can suggest for those results is, first, the modification of the electronic attachment and photon absorption by the formation of water clusters and aggregates at high humidity levels. Stronger attachment and absorption rates may change both the distribution of the electric field in the discharge (with lower fields at the front and higher ones near the pin) and the extent of the photo-ionization. With high electron affinities and lower ionization energies than single water molecules, clusters can also directly change the energy distribution function of electrons by preventing some of them to reach high energy levels or by creating new electrons in the highest field part of the discharge. The second point concerns the role of the ions on the very fast heating of the gas. Their mobility in the very strong fields close to the pin could be high enough to transfer some of their energy significantly. At later times in the early post discharge, the same humidity threshold effect

on gas heating is accentuated and clear, as will be presented in a future work.

Diffuse discharges at atmospheric pressure present a new route for applications needing large plasma volumes and high densities of reactive species, even in humid environments. For instance, the combination of a large, diffuse plasma and high electric fields could be used for the treatment of gas effluents, assisted combustion or for exsitu biomedical applications for which the plasma usually interacts with wet surfaces and for which the water vapour affects in turn the discharge.

7. Acknowledgments

This work was supported by the French National Research Agency, ANR-13-BS09-0014 (EXFIDIS) research program. The authors are thankful to Dr Jean-Pascal Borra for fruitful discussion about discharge-aerosols interaction.

8. References

[1] Naidis G V, Tarasenko V F, Babaeva N Yu and Lomaev M I 2018 Subnanosecond breakdown in high-pressure Gases *Plasma Sources Sci. Technol.* **27 013001**
[2] Teunissen J and Ebert U 2016 3D PIC-MCC simulations of discharge inception around a sharp anode in nitrogen/oxygen mixtures *Plasma Sources Sci. Technol.* **25 044005**
[3] Chen S, Heijmans L C J, Zeng R, Nijdam S and Ebert U 2015 Nanosecond repetitively pulsed discharges in N2-O2 mixtures: inception cloud and streamer emergence *J. Phys. D: Appl. Phys.* **48 175201**
[4] Tardiveau P, Magne L, Marode E, Ouaras K, Jeanney P and Bournonville B 2016 Sub-nanosecond time resolved light emission study for diffuse discharges in air under steep high voltage pulses *Plasma Sources Sci. Technol.* **25 054005**
[5] Tarasenko V F, Naidis G V, Beloplotov D V, Kostyrya I D, Babaeva N Yu 2018 Formation of Wide Streamers during a Subnanosecond Discharge in Atmospheric-Pressure Air *Plasma Physics Reports* **44, 8 746–753**
[6] Raizer Y P 1991 Gas Discharge Physics (Berlin: Springer)
[7] Cernák M, Hoder T and Bonaventura Z 2020 Streamer breakdown: cathode spot formation, Trichel pulses and cathode-sheath instabilities *Plasma Sources Sci. Technol.* **29 013001**
[8] Babaeva N Yu and Naidis G V 2016 Modeling of streamer dynamics in atmospheric-pressure air: influence of rise time of applied voltage pulse on streamer parameters *IEEE Trans. Plasma Sci.* **44 899–902**
[9] Komuro A, Ono R and Oda T 2013 Effects of pulse voltage rise rate on velocity, diameter and radical production of an atmospheric-pressure streamer discharge *Plasma Sources Sci. Technol.* **22 045002**
[10] Pai D Z, Stancu G D, Lacoste D A and Laux C O 2009 Nanosecond repetitively pulsed discharges in air at atmospheric pressure - the glow regime *Plasma Sources Sci. Technol.* **18 045030**
[11] Stepanyan S, Starikovskiy A Y, Popov N and Starikovskaia S 2014 A nanosecond surface dielectric barrier discharge in air at high pressures and different polarities of applied pulses: transition to filamentary mode *Plasma Sources Sci. Technol.* **23 045003**
[12] Nudnova M M and Starikovskii A Yu 2008 Development of streamer flash initiated by HV pulse with nanosecond rise time *IEEE Trans. Plasma Sci.* **36, 4 896-897**
[13] Tarasenko V F 2014 Runaway Electrons Preionized Diffuse Discharges (New York: Nova Science)
[14] Babaeva N Yu, Naidis G V, Tereshonok D V and Son E E 2018 Development of nanosecond discharges in atmospheric pressure air: two competing mechanisms of precursor electrons production *J. Phys. D: Appl. Phys.* **51 434002**
[15] Kostyrya I D and Tarasenko V F 2010 Soft X Ray Radiation Due to a Nanosecond Diffuse Discharge in Atmospheric Pressure Air *Technical Physics* **55, 2 270–276**
[16] Kozyrev A V, Tarasenko V F, Baksht E K and Shut'ko Y V 2011 Soft x-ray generation and its role in breakdown of air gap at elevated pressures *Tech. Phys. Lett.* **37 1054–7**
[17] Babich L P 2003 High-Energy Phenomena in Electric Discharges in Dense Gases: Theory, Experiment and Natural Phenomena (Arlington, VA: Futurepast)

[18] Marode E, Dessante Ph and Tardiveau P 2016 2D positive streamer modelling in NTP air under extreme pulse fronts. What about runaway electrons? *Plasma Sources Sci. Technol.* **25 064004**
[19] Köhn C, Chanrion O and Neubert T 2017 The influence of Bremsstrahlung on electric discharge streamers in N2, O2 gas mixtures *Plasma Sources Sci. Technol.* **26 015006**
[20] Levko D and Raja L L 2015 Dynamics of a wire-to-cylinder atmospheric pressure high-voltage nanosecond discharge *Phys. Plasmas* **22 083507**
[21] Chng T L, Brisset A, Jeanney P, Starikovskaia S M, Adamovich I V and Tardiveau P 2019 Electric field evolution in a diffuse ionization wave nanosecond pulse discharge in atmospheric pressure air *Plasma Sources Sci. Technol.* **28 09LT02**
[22] Brisset A, Gazeli K, Magne L, Pasquiers S, Jeanney P, Marode E and Tardiveau P 2019 Modification of the electric field distribution in a diffuse streamer-induced discharge under extreme overvoltage *Plasma Sources Sci. Technol.* **28 055016**
[23] Ouaras K, Magne L, Pasquiers S, Tardiveau P, Jeanney P and Bournonville B 2018 OH density measured by PLIF in a nanosecond atmospheric pressure diffuse discharge in humid air under steep high voltage pulses *Plasma Sources Sci. Technol.* **27 045002**
[24] Bentaleb S, Tardiveau P, Moreau N, Jeanney P, Jorand F, and Pasquiers S 2011 Filamentation of a nanosecond pulse corona
discharge in air-propane mixtures at atmospheric pressure *IEEE Trans. Plasma Sci.* **39 2236-2237**
[25] Allen N L, Fonseca J R, Geldenhuys H J and Zheng J C 1991 Humidity influence on non-uniform field breakdown in air *Electra* **134 63-89**
[26] Fenger M and Stone G C 2005 Investigations into the effect of humidity on stator winding partial discharges *IEEE Trans. Dielectrics and Electrical Insulation* **12, 2 341-346**
[27] Mikropoulos P N and Stassinopoulos C A 1998 Humidity effect on the properties of coronas preceding breakdown in short positive rod - plane gaps *33rd Universities Power Engineering Conference* **69** (Edinburgh, UK)
[28] Davies A J, Dutton J, Turri R and Waters R T 1988 Effect of humidity and gas-density on switching impulse breakdown of short airgaps *IEE Proceedings A Science Measurement and Technology* **135, 1 59-68**
[29] Allen N L, Berger G, Dring D, Hahn R 1981 Effects of humidity on corona inception in a diverging electric-field *IEE Proceedings A Science Measurement and Technology* **128, 8 565-570**
[30] Ortéga P, Díaz R, Heilbronner F and Rühling F 2007 Influence of negative ions on the humidity effect on the first corona inception *J. Phys. D: Appl. Phys.* **40 7000–7007**
[31] Mikropoulos P N, Stassinopoulos C A and Sarigiannidou B C 2008 Positive streamer propagation and breakdown in air: the influence of humidity *IEEE Trans. Dielectrics and Electrical Insulation* **15, 2 416-425**
[32] Meng X, Mei H, Wang L, Guan Z and Zhou J 2017 Characteristics of streamer propagation along the insulation surface: Influence of air pressure and humidity *IEEE Trans. Dielectrics and Electrical Insulation* **24, 1 391-400**
[33] Gallimberti I 1979 The mechanism of the long spark formation *J. Phys. Colloques* **40 C7-193-C7-250**
[34] Phelps C T and Griffiths R F 1976 *J. Appl. Phys.* **47 2929**
[35] Aleksandrov N L and Bazelyan E M 1999 *Plasma Sources Sci. Technol.* **8 285**
[36] Marr G 1967 Photoionization processes in gases (New York: Academic Press)
[37] Komuro A and Ono R 2014 Two-dimensional simulation of fast gas heating in an atmospheric pressure streamer discharge and humidity effects *J. Phys. D: Appl. Phys.* **47 155202**
[38] Aleksandrov N L and Bazelyan E M 1996 Temperature and density effects on the properties of a long positive streamer in air *J. Phys. D: Appl. Phys.* **29, 11 2873-2880**
[39] Komuro A, Matsuyuki S and Ando A 2018 Simulation of pulsed positive streamer discharges in air at high temperatures *Plasma Sources Sci. Technol.* **27 105001**
[40] Schneider K H 1977 Positive discharges in long air gaps at Les Renardières *Electra* **53 33-153**
[41] Sieck L W, Herron J T and Green D S 2000 Chemical Kinetics Database and Predictive Schemes for Humid Air Plasma Chemistry. Part I: Positive Ion–Molecule Reactions *Plasma Chemistry and Plasma Processing* **20 235-258**
[42] Popov N A 2011 Fast gas heating in a nitrogen-oxygen discharge plasma: I. Kinetic mechanism *J. Phys. D: Appl. Phys.* **44 285201**

[43] N L Aleksandrov N L, Kindysheva S V, Nudnova M M and Starikovskiy A Yu 2010 Mechanism of ultra-fast heating in a non-equilibrium weakly ionized air discharge plasma in high electric fields *J. Phys. D: Appl. Phys.* **43 255201**
[44] Moreau N, Decharge nanoseconde dans l'air et en melange air / propane. Application au declenchement de combustion, *2011, Paris 11*
[45] Beniaminy I, Deutsch M 1982 Abel: stable, high accuracy program for the inversion of Abel's integral equation *Computer Physics Communications* **27** 415—422
[46] Cardoso R P, Belmonte T, Keravec P, Kosior F and Henrion G 2007 Influence of impurities on the temperature of an atmospheric helium plasma in microwave resonant cavity *J. Phys. D: Appl. Phys.* **40 1394**
[47] Gazeli K, Svarnas P, Held B, Marlin L and Clement F 2015 Possibility of controlling the chemical pattern of He and Ar "guided streamers" by means of N_2 or O_2 additives *J. Appl. Phys.* **117 093302**
[48] Voráč J, Synek P, Potočňáková L, Hnilica J and Kudrle V 2017 Batch processing of overlapping molecular spectra as a tool for spatio-temporal diagnostics of power modulated microwave plasma jet *Plasma Sources Science and Technology* **26(2) 025010**
[49] Voráč J, Synek P, Procházka V and Hoder T 2017 State-by-state emission spectra fitting for non-equilibrium plasmas: OH spectra of surface barrier discharge at argon/water interface *Journal of Physics D: Applied Physics* **50(29) 294002**
[50] Brau C A and Jonkman RM 1970 Classical theory of rotational relaxation in diatomic gases *J. Chem. Phys.* **52 477–84**
[51] Lofthus A and Krupenie P H 1977 The spectrum of molecular nitrogen *Journal of Physical and Chemical Reference data* **6 113-307**
[52] Kossyi I A, Kostinsky A Yu, Matveyev A A and Silakov V P 1992 Kinetic scheme of the non-equilibrium discharge in nitrogen-oxygen mixtures *Plasma Sources Sci. Technol.* **1 207**
[53] Rusterholtz D L, Lacoste D A, Stancu G D, Pai D Z and Laux C O 2013 Ultrafast heating and oxygen dissociation in atmospheric pressure air by nanosecond repetitively pulsed discharges *J. Phys. D: Appl. Phys.* **46 464010**
[54] Park C 1989 Nonequilibrium Hypersonic Aerothermodynamics (New York: Wiley)
[55] Brisset A, Guichard F, Cessou A, Tardiveau P Energy relaxation and heating in the afterglow of high field ns-discharges in ambient air using spontaneous Raman scattering *Plasma Sources Sci. and Tech. (under submission)*
[56] Itikawa Y and Mason N 2005 Cross sections for electron collisions with water molecules *Journal of Physical and Chemical Reference Data* **34 1**
[57] Makogon M M, Ponomarev Yu N and Tikhomirov B A 2013 The problem of water vapor absorption in the UV spectral range *Atmospheric and Oceanic Optics* **26, 1 45–49**
[58] Märk T D 1991 Free electron attachment to Van der Waals clusters *International Journal of Mass Spectrometry and Ion Processes* **107 143-163**
[59] Belau L, Wilson K R, Leone S R and Ahmed M 2007 Vacuum ultraviolet (VUV) photoionization of small water clusters *J. Phys. Chem. A* **111 10075-10083**
[60] Mota R, Parafita R, Giuliani A, Hubin-Franskin M-J, Lourenço J.M.C, Garcia G, Hoffmann S V, Mason N J, Ribeiro P A, Raposo M and Limão-Vieira P 2005 Water VUV electronic state spectroscopy by synchrotron radiation *Chemical Physics Letters* **416 152-159**
[61] Wozniak B and Dera J 2007 Light Absorption in Sea Water (New-York: Springer)
[62] Tsuchiya M, Tashiro T, Shigihara A, 2004 *J. Mass Spectrom. Soc. Jpn.* **52 1**
[63] Borra J-P, Goldman A, Goldman M and Boulaud D 1998 Electrical discharge regimes and aerosol production in point-to-plane DC high pressure cold plasmas: aerosol production by electrical discharges *J. aerosol Sci.* **29 661-674**
[64] Borra J-P, Jidenko N, Hou J and Weber A 2015 Vaporization of bulk metals into single-digit nanoparticles by non-thermal plasma filaments in atmospheric pressure dielectric barrier discharges *J. Aerosol Sci***. 79 109-125**
[65] Borra J-P 2018 Review on water electro-sprays and applications of charged drops with focus on the corona-assisted cone-jet mode for High Efficiency Air Filtration by wet electro-scrubbing of aerosols. *J. Aerosol Sci***. 125**

208-236
[66] Hagelaar G J M and Pitchford L C 2005 Solving the Boltzmann equation to obtain electron transport coefficients and rate coefficients for fluid models *Plasma Sci. Sources and Tech.* **14, 722**
[67] Database https://cccbdb.nist.gov/
[68] Segarra-Martí J, Merchán M and Roca-Sanjuán D 2012 Ab initio determination of the ionization potentials of water clusters $(H_2O)n$ (n = 2−6) *J. Chem. Phys.* **136 244306**